ACS APPLIED MATERIALS & INTERFACES

www.acsami.org

Research Article

Dressing Blood-Contacting Materials by a Stable Hydrogel Coating with Embedded Antimicrobial Peptides for Robust Antibacterial and Antithrombus Properties

Kunpeng Liu,[#] Fanjun Zhang,[#] Yuan Wei, Qinsheng Hu, Qingfeng Luo, Chong Chen, Jingyu Wang, Li Yang,* Rifang Luo,* and Yunbing Wang

Cite This: *ACS Appl. Mater. Interfaces* 2021, 13, 38947−38958

Read Online

ACCESS | Metrics & More | Article Recommendations | Supporting Information

ABSTRACT: Although dressing blood-contacting devices with robust and synergistic antibacterial and antithrombus properties has been explored for several decades, it still remains a great challenge. In order to endow materials with remarkable antibacterial and antithrombus abilities, a stable and antifouling hydrogel coating was developed via surface-initiated polymerization of sulfobetaine methacrylate and acrylic acid on a polymeric substrate followed by embedding of antimicrobial peptides (AMPs), including WR (sequence: WRWRWR-NH_2) or Bac2A (sequence: RLARIVVIRVAR-NH_2) AMPs. The chemical composition of the AMP-embedded hydrogel coating was determined through XPS, zeta potential, and SEM−EDS measurements. The AMP-embedded antifouling hydrogel coating showed not only good hemocompatibility but also excellent bactericidal and antiadhesion properties against Gram-positive and Gram-negative bacteria. Moreover, the hydrogel coating could protect the AMPs with long-term bioactivity and cover the positive charge of the dotted distributed AMPs, which in turn well retained the hemocompatibility and antifouling capacity of the bulk hydrogels. Furthermore, the microbiological results of animal experiments also verified the anti-infection performance in vivo. Histological and immunological data further indicated that the hydrogel coating had an excellent anti-inflammatory function. Therefore, the present study might provide a promising approach to prevent bacterial infections and thrombosis in clinical applications of blood-contacting devices and related implants.

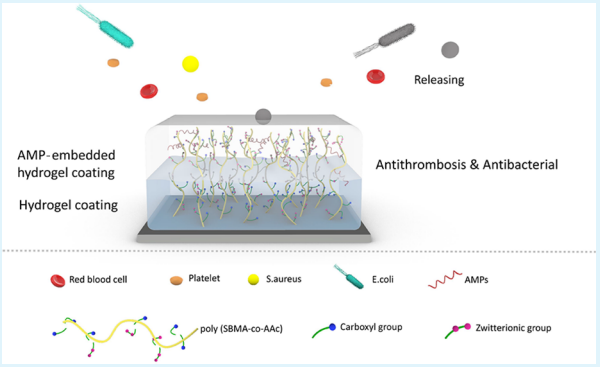

KEYWORDS: *antimicrobial peptides, hydrogel coating, hemocompatibility, antibacterial, blood-contacting devices*

1. INTRODUCTION

As two major clinical complications of blood-contacting devices and related implants, bacterial infection and thrombosis cause device or implant failure, patient morbidity, mortality, and increasing healthcare costs.[1−3] Once the devices are exposed to the blood, they would trigger clotting, leading to clot formation or an immune response. If the clot breaks off and travels with the blood to the lungs, brain, or other organs, systemic complications occur and endanger the life of the patient, such as cerebral infarction and pulmonary embolism.[4] Therefore, it is very important to investigate the antithrombotic activities of blood-contacting medical devices. Coadministration of antibiotics and anticoagulant drugs is a well-recognized strategy to reduce these two complications. However, this might pose risks of emergence of antibiotic-resistant microbes and major bleeding.[5−7] To address these problems, dressing blood-contacting devices or implants with in situ or localized antibacterial and antithrombus properties is considered as a promising approach.[8,9]

Generally, surface functionalization to reduce bacterial infections mainly focuses on the construction of a surface with bactericidal[10−12] and antifouling[13−16] properties. The bactericidal surface could be achieved via various strategies, including doping of metal ions,[17−21] coating of antibiotics,[22−24] and conjugation of cationic polymers.[25−27] The antifouling surface could be achieved by modification with hydrophilic polymers, such as polyethylene glycol and zwitterionic polymers.[28−30] A hydration layer could be easily generated on a hydrophilic surface due to the interaction between water and hydrophilic components, thus reducing the nonspecific adsorption of proteins or bacteria onto the surface.

Received: March 19, 2021
Accepted: August 6, 2021
Published: August 16, 2021

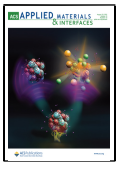

More importantly, the antifouling surface is also efficient for thrombus resistance by reducing the absorption and activation of platelets and fibrins. However, it is hard for the surface with an individual antifouling function to prevent the colonization and growth of bacteria for a long period.[31,32] In addition, the antifouling surface could not inactivate bacteria, leading to infection in the bloodstream or other locations.[33] Moreover, the bactericidal surface also exhibits some disadvantages, including a short lifetime, cumulative toxicity, and poor hemocompatibility, which limits its application in blood-related medical devices.[34−38] Therefore, single-functional surfaces with antifouling or bactericidal properties alone are insufficient in clinical applications. Nowadays, an increasing attention has been focused on developing dual-functional surfaces with integrated antifouling and bactericidal properties.[8,39,40]

Among the reported antibiotics, antimicrobial peptides (AMPs) are a kind of a peptide substance that naturally exists in organisms as an important part of innate immunity. Such active peptides are generally cationic short peptides consisting of 5−100 amino acid residues with molecular weights between 1 and 5 kDa.[41,42] AMPs exhibit a broad-spectrum antibacterial function and an amphiphilic structure. Owing to the presence of cations, AMPs could destroy the bacterial cell membrane and kill bacteria through preferentially combining with the negative parts of the cell membrane and inserting the hydrophobic end into the phospholipid molecular layer.[43] Thereby, AMPs have been widely studied and considered to be a valuable drug with ideal antibacterial properties. Many researchers have attempted to apply AMPs for surface modification; unfortunately antimicrobial activities are greatly reduced when AMPs are immobilized onto the surface directly.[44] Furthermore, proteins and the dead bacteria may be easily adsorbed due to the cationic nature of AMPs, which can further trigger an immune response and inflammation as well as block the antimicrobial functional groups.[45,46] More importantly, if platelets are adsorbed and activated, risks of thrombus and red blood cell hemolysis might be enhanced, which significantly restricts the application in blood-contacting devices or implants.[47]

Among the current strategies, surface grafting of hydrophilic polymers or fluoride molecules could decrease the risk of thrombus formation and bacterial infection. Among them, a hydrogel coating possesses unique advantages. The typical "soft and wet" properties of hydrogels are very similar to biological tissues and have been widely used in a variety of biomedical fields. However, poor mechanical properties of most hydrogels hamper their application, especially in biomedical devices such as catheters that need to be inserted into the body. Coating a thin layer of hydrogel on the surface of devices is an effective way to overcome these disadvantages and endow the device with superior biocompatibility.[48−50]

To achieve the dual function of antibacterial and antithrombus properties, herein, we put forward a strategy to develop an AMP-embedded hydrogel coating, where the embedded AMPs were expected to endow the hydrogel coating with antibacterial properties and the hydrogel coating was expected to retain its good antithrombus and antifouling properties. In this study, a surface-initiated polymerization method was performed to achieve a robust hydrogel coating on a polymer substrate, and sulfobetaine methacrylate (SBMA) and acrylic acid (AAc) were chosen as the hydrogel monomers to achieve good hemocompatibility. Two kinds of AMPs (WR (sequence: WRWRWR-NH_2) or Bac2A (sequence: RLAR-IVVIRVAR-NH_2)) with different numbers of amino acid residues were embedded in the hydrogel coating using a chemical grafting method to achieve antibacterial properties. The chemical structure of the AMP-embedded hydrogel coating was determined using X-ray photoelectron spectroscopy (XPS), zeta potential, and scanning electron microscopy−energy-dispersive X-ray spectroscopy (SEM−EDS) measurements, and the hemocompatibility and antibacterial properties were evaluated with ex vivo, in vivo, and in vitro techniques.

2. EXPERIMENTAL SECTION

2.1. Materials and Reagents. A polyvinyl chloride (PVC) tube was obtained from Shanxi Jingdian Biological Technology Co. Ltd. (Shanxi, China) with an approximate size of 5.3 mm in inner diameter. 3-[Dimethyl-[2-(2-methylprop-2-enoyloxy)ethyl]-azaniumyl]propane-1-sulfonate (SBMA) and AAc were purchased from Sigma-Aldrich. Benzophenone, *N*-hydroxysuccinimide (NHS), 1-(3-dimethylaminopropyl)-3-ethylcarbodiimide hydrochloride (EDC), and toluidine blue were purchased from Aladdin Bio-Chem Technology Co. Ltd. (Shanghai, China). AMPs (WR (sequence: WRWRWR-NH2) and Bac2A (sequence: RLARIVVIRVAR-NH2)) were obtained from Hangzhou Allpeptide Biotechnology Co. Ltd. (Hangzhou, China). Bacterial media and agar were purchased from Basebio (China). The cell counting kit-8 (CCK-8) was obtained from Dojindo Technology Co. Ltd. (Beijing, China). A lactate dehydrogenase (LDH) cytotoxicity assay kit was obtained from Beyotime Biotechnology Co. Ltd. (Shanghai, China). The LIVE/DEAD BacLight bacterial viability kit (L-7007, Invitrogen) was purchased from Thermo Fisher Scientific Co. Ltd. (Shanghai, China). The bacterial strains of *Escherichia coli* (*E. coli*, ATCC 25922) and *Staphylococcus aureus* (*S. aureus*, ATCC 25923) were obtained from Bena Culture Collection (Beijing, China).

2.2. Preparation of the Hydrogel Coating. The PVC tube was washed several times with water and ethanol before the usage followed by filling with benzophenone acetone solution (20 wt %) for 15 min. After draining the solution, the PVC tube was filled with a monomer aqueous solution (10 wt %, SBMA/AAc = 3:7 molar ratio) and irradiated under UV (CL-1000L, UVP, USA) at 365 nm. After 1 h, a hydrogel coating formed on the tube surface and the residual monomer aqueous solution was drained. Then, the tube was immersed into a saturated sodium carbonate solution to convert carboxyl groups (−COOH) into $-COO^-Na^+$. Finally, the hydrogel-coated PVC tube was immersed into water for 3 days to remove all the residual monomers before drying at room temperature. The hydrogel coating grafted with poly(SBMA-co-AAc) inside the tube surface was obtained and denoted as SA.

Conventional EDC/NHS chemistry was applied to prepare the AMP-embedded hydrogel coating. First, the SA tube was activated in a MES solution (pH 5.5) containing 0.4 M EDC and 0.1 M NHS at 4 °C for 1 h. The activated tube was then treated with a solution of Bac2A or WR (5 mg/mL) in PBS (pH 7.4) at 4 °C for 24 h. The AMP-tethered tubes were washed with water, dried with a stream of nitrogen, and stored at 4 °C. The amount of AMPs loaded in the hydrogels was determined by the concentration difference before and after AMP grafting, and the concentration of the AMPs was determined by high-performance liquid chromatography as we previously reported.[48] The hydrogel coating grafted with AMPs WR (amino acid sequence: WRWRWR-NH_2) and Bac2A (amino acid sequence: RLARIVVIRVAR-NH_2) was named as SA-WR and SA-Bac2A, respectively.

2.3. Characterization of the Hydrogel Coating. The cover area ratio of the hydrogel coating on the tube surface was identified by staining with toluidine blue. Typically, the hydrogel-coated PVC tube was immersed into a toluidine blue aqueous solution (10 mg/mL) for 1 h and then washed with water for another 3 h to remove any unbonded dye. The positively charged toluidine blue could stain

https://doi.org/10.1021/acsami.1c05167
ACS Appl. Mater. Interfaces 2021, 13, 38947−38958

hydrogels through a reaction with the negatively charged carboxyl groups in the hydrogel coating.

Surface morphology and the thickness of the hydrogel coating were observed using a field-emission scanning electron microscope (Nova NanoSEM 450, FEI, USA).

The thicknesses of the hydrogel coating before and after water absorption were also determined using an optical microscope (NM910-TR, Nexcope, CN).

The wettability of the hydrogel coating was evaluated using a water contact angle analyzer (WCA, Theta Lite, Biolin Scientific, Sweden). A volume of 5 μL of water was dropped onto the sample surface with a size of 1 × 1 cm^2 to obtain the static contact angle. Another 5 μL of water was dropped onto the sample surface at the same location to obtain the advancing contact angle, which was then absorbed away to obtain the receding contact angle.

The surface zeta potential was measured at pH 7.4 in 0.1 mM KCl solution with an adjustable gap cell (SurPASS 3, Anton Paar, Austria).

The chemical composition of the hydrogel coating was determined using an attenuated total reflection−Fourier transform infrared (ATR-FTIR) spectrometer (Nicolet iS10, Thermo Fisher Scientific, USA), an X-ray photoelectron spectrometer (XPS) equipped with an Al Kα achromatic X-ray source (Escalab 250Xi, Thermo Fisher Scientific, USA) with a take-off angle of 90°, and an energy-dispersive X-ray spectrometer (EDS, Ultim Max 100, Oxford, UK).

To evaluate the hydrogel coating stability, the residual mass of the sample was tested after immersing into phosphate-buffered saline (PBS) at 37 °C with shaking for several weeks.

2.4. Blood Compatibility. *2.4.1. Platelet Adhesion Test.* Whole blood was collected from a rabbit in negative pressure tubes containing sodium citrate (109 mmol/L) as the anticoagulant. The exact ratio of blood collected to the anticoagulant was 9:1. Prior to platelet adhesion and activation tests, the platelet-rich plasma (PRP) was obtained by centrifuging the whole blood at 1500 rpm for 15 min. All the samples were incubated with PRP at 37 °C for 1 h, washed with physiological saline (0.9 wt %) for 15 min, and then fixed with 2.5% glutaraldehyde solution for 12 h at 4 °C; then, the samples were rinsed with PBS for three times to remove glutaraldehyde solution and completely immersed in 30, 50, 70, 90, and 100 wt % ethanol solutions (ethanol:water) in turn for 15 min each time. The morphology of the adherent platelets on PVC without/with the coating was observed using a SEM with the pretreatment of gold spray.

Additionally, an LDH assay was performed to semi-quantitatively analyze platelet adhesion. LDH was released from platelets, which could be used to evaluate the number of platelets adhered to the surface. The whole test of the LDH assay process was conducted based on the instruction manual. In brief, samples were incubated with PRP at 37 °C for 1 h. Next, samples were removed from PRP and rinsed with PBS for three times (to remove platelets that did not adhere). Samples were incubated with an "LDH release solution" provided by the LDH assay kit at 37 °C for 1 h. After this, the supernatant liquid of the samples was added to new 96-well plates and an "LDH working solution" was added and mixed with the supernatant liquid; then, the mixture solution was incubated under dark conditions for 0.5 h. Finally, the absorbance of each mixture solution was measured at 490 nm. The LDH activity of the platelet was evaluated using the optical value (OD).

2.4.2. Hemolysis and Cytotoxicity Assays. The hemolysis ratio was determined according to the reported method.[51] Each sample was cut into a 1.5 cm × 1 cm piece and suspended in 1 mL of PBS with 5% red blood cells (RBCs) for 2 h at 37 °C. Pure water with 5% RBCs and PBS with 5% RBCs acted as a positive control and a negative control in the experiment, respectively. After incubation for 2 h, 100 μL of the supernatant after centrifugation was pipetted into a 96-well plate and the absorbance was determined at 541 nm with a microplate reader (Synergy H1, BioTek Instruments Inc.). The hemolysis ratio was calculated with the following equation.

$$\text{hemolysis ratio (\%)} = \frac{A_{\text{sample}} - A_{\text{negative}}}{A_{\text{positive}} - A_{\text{negative}}} \times 100$$

2.4.3. Ex Vivo Blood Circulation. All of the animal experiments were performed in compliance with the guidelines issued by the Ethical Committee of the Chinese Academy of Sciences (CAS) and approved by the Ethical Committee of CAS. The experimental animals were purchased from Chengdu Dashuo Experimental Animal Co., Ltd. (Chengdu, China). New Zealand white rabbits (2.5−3.0 kg) were used for the ex vivo blood circulation test and anesthetized with pentobarbital sodium. The ex vivo antithrombogenicity assay was performed according to the reported procedure.[52] An ex vivo blood circuit was built by connecting the blood vessels with a PVC catheter having SA, SA-WR, and SA-Bac2A. After operation for 2 h, the samples were removed and rinsed with physiological saline (0.9 wt %) for three times. Then, the surface morphology of the sample was observed with a SEM after fixation, dehydration, and dealcoholization.

2.5. Antibacterial and Antifouling Properties. *S. aureus* (ATCC 6538) and *E. coli* (ATCC 25922) as the common microorganisms involved in hospital-acquired infections were used to evaluate the antibacterial and antifouling properties of the hydrogel coating.

To evaluate the antibacterial properties of the hydrogel coatings, PVC, SA, SA-WR, and SA-Bac2A samples were cut into 1.0 cm × 1.0 cm pieces and then 80 μL of sterilized PBS containing 1 × 10^6 CFU/mL of *E. coli* and *S. aureus* was added, respectively. In order to prevent the evaporation of liquid, all the samples were covered with sterile polyethylene films and then incubated at 37 °C in a constant temperature incubator. After 6 h, the samples with the bacterial suspension and polyethylene films were put into tubes together with 1 mL of sterilized PBS and ultrasonicated for 5 min to elute the live bacteria. Finally, 100 μL of the bacterial suspension was inoculated in a medium of nutrient agar and incubated at 37 °C for 12 h, and the numbers of colonies were counted to determine the antibacterial properties.

To evaluate the long-term antibacterial activity of the hydrogel coatings, AMP, PVC, SA, SA-WR, and SA-Bac2A samples were immersed into PBS at 37 °C with shaking for 4 weeks or stored under dry conditions for 4 weeks, and the antibacterial ability was tested with the same method as described above.

To evaluate the antifouling ability of the hydrogel coatings, PVC, SA, SA-WR, and SA-Bac2A samples were cut into 0.8 cm × 0.8 cm pieces and incubated in an MH medium containing 1 × 10^8 CFU/mL of *E. coli* and *S. aureus*, respectively. After incubation at 37 °C for 12 h, the samples were gently rinsed with normal saline solution for three times. Then, the samples were soaked into a staining solution containing SYTO 9 and propidium iodide from a live/dead staining kit in the dark and observed with a confocal laser scanning microscope (CLSM, Leica TCS SP5, Germany).

2.6. Cell Viability of the Hydrogel Coating. To evaluate the biocompatibility of the hydrogel coatings, the leaching liquor effect of the samples on the growth of human umbilical vein endothelial cells (HUVECs) was studied. First, samples were sterilized with 75% ethanol for 2 h and then immersed in 0.5 mL of RPMI-1640 medium for another 24 h. The ratio of the sample to RPMI-1640 medium was 3 cm^2/mL. The extract was then diluted to a series of concentrations for the cytotoxicity test. HUVECs after two passage times were seeded in a 96-well plate in triplicate at a density of 8000 cells per well. After 24 h, the culture medium was removed and then 100 μL of the extract was added for another 24 h of culture. The cell viability cultured in tissue-culture polystyrene with a fresh culture medium is defined as 100%. The cell viability was evaluated using the CCK-8 assay kit as previously reported.[52,53]

2.7. In Vivo Biocompatibility and Anti-Infection Evaluation. Male Sprague−Dawley (SD) rats aged 8 weeks with a body weight of around 200 g were used for the in vivo anti-infection assay. Surgical operations were performed after 1 week of adaption. SD rats were anesthetized using chloral hydrate, and the hair on the operating sites was shaved. Then, two incisions with a length of 10 mm were cut parallel to the spine. PVC, SA, SA-WR, and SA-Bac2A samples (0.8

https://doi.org/10.1021/acsami.1c05167
ACS Appl. Mater. Interfaces 2021, 13, 38947−38958

Scheme 1. Schematic Illustration of the AMP-Embedded Hydrogel Coating Preparation inside PVC Tubes

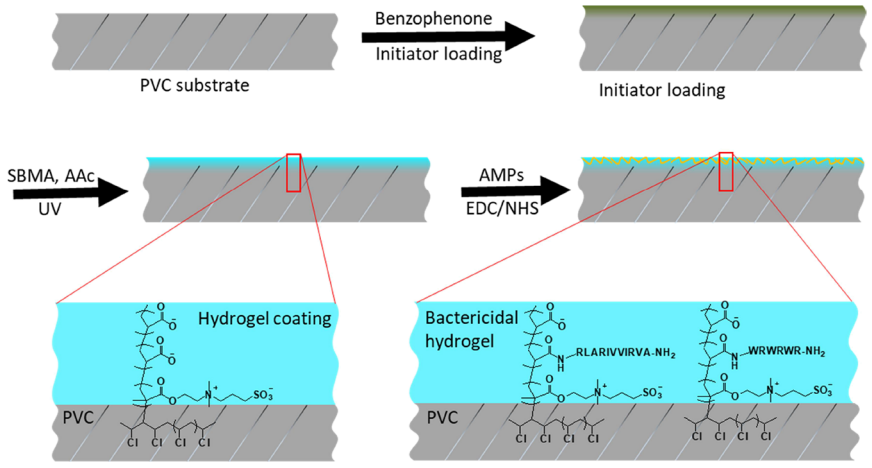

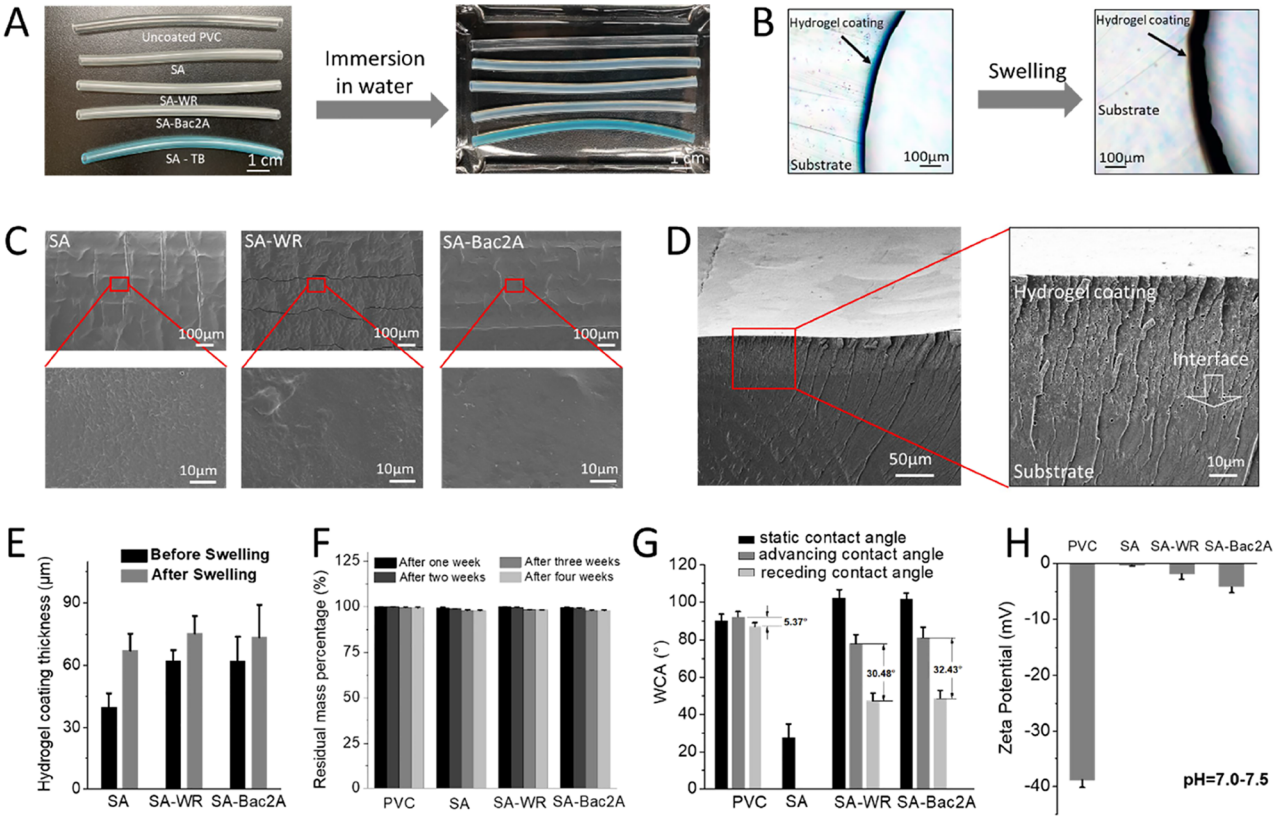

Figure 1. (A) Optical images of tubes, from top to down: uncoated PVC tube, SA (poly(SMBA-co-AAc) hydrogel coating), SA-WR (the hydrogel coating grafted with AMP WR (amino acid sequence: WRWRWR-NH2)), SA-Bac2A (the hydrogel coating grafted with AMP WR (amino acid sequence: RLARIVVIRVAR-NH_2)), and SA-TB (the SA hydrogel coating stained by toluidine blue). (B) Microphotograph of the sectional view of the SA hydrogel coating stained by toluidine blue; the left image was recorded under dry conditions, and the right was recorded under swelling conditions. (C) Surface SEM images of SA, SA-WR, and SA-Bac2A hydrogel coatings. (D) Cross-sectional SEM images of the SA hydrogel coating. (E) Thickness of the hydrogel coating before and after water absorption (mean values ± SD, n = 3). (F) Residual mass percentage (%) of samples after 4 weeks, and samples were immersed into PBS with shaking for 4 weeks (mean values ± SD, n = 4) (G) WCA of the hydrogel coating, including static, advancing, and receding contact angles (mean values ± SD, n = 3). (H) Surface zeta potential of the hydrogel coating (mean values ± SD, n = 3).

cm × 0.8 cm) were implanted into the back of the SD rats, and then 100 μL of *S. aureus* suspension (1 × 10^6 CFU/mL) was injected on the coating surface of tubes. The incisions were closed with 4−0 sutures. After 1 or 3 days, the rats were humanely euthanized, and the implanted samples were harvested. All implanted samples were collected and immersed into 2 mL of PBS. After ultrasonic cleaning, 100 μL of the suspension was used for the spread plate method. Soft tissues around the samples were collected, fixed, and then stained with hematoxylin−eosin (H&E). Meanwhile, immunohistochemical staining was performed to evaluate the inflammatory reaction. Mouse antirat CD68 antibody and rabbit antirat CD3 antibody were used to label the macrophage cells and T cells, respectively.

2.8. Statistical Analysis. All the quantitative results were expressed as mean ± standard deviation (SD). Each assay was

https://doi.org/10.1021/acsami.1c05167
ACS Appl. Mater. Interfaces 2021, 13, 38947−38958

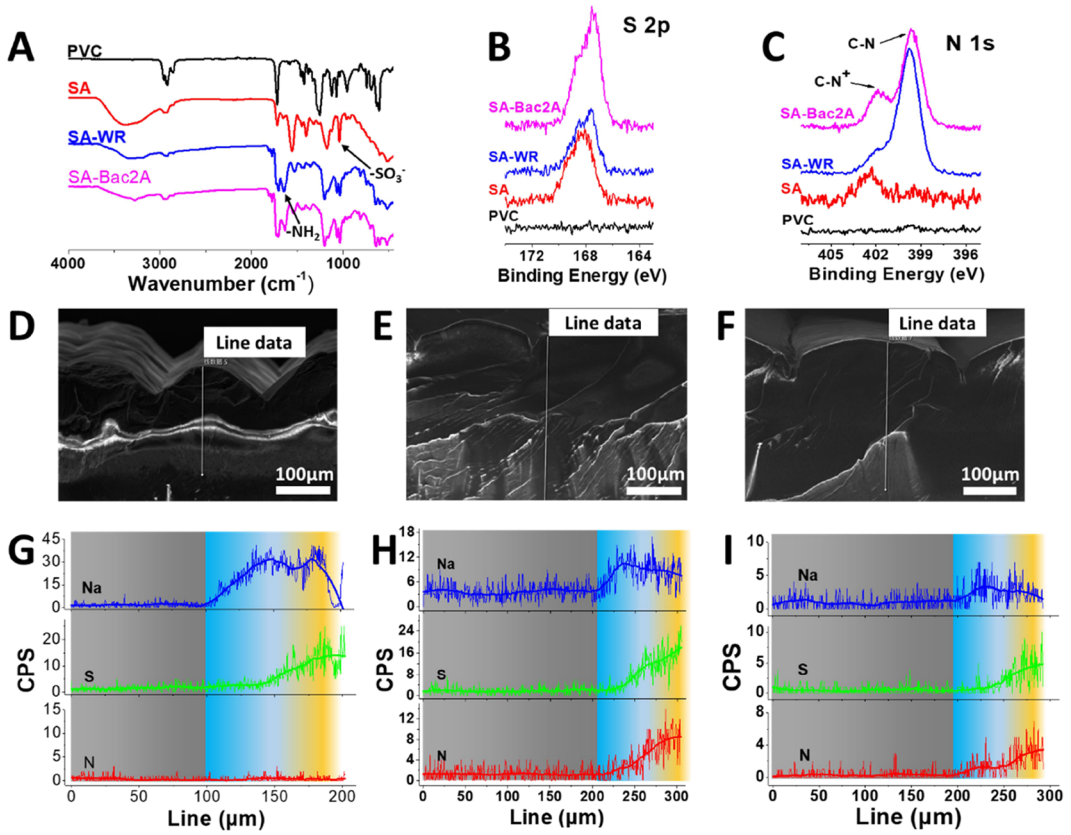

Figure 2. (A) FTIR spectra of PVC, SA, SA-WR, and SA-Bac2A. (B, C) XPS spectra of S 2p and N 1s of PVC, SA, SA-WR, and SA-Bac2A. (D–F) SEM images of the cross-sectional view of SA (D), SA-WR (E), and SA-Bac2A (F), respectively. The data in panels (G–I) represent the element distribution of Na, S, and N along with the white line in panels (D–F). The color background depicts the chemical structure of samples in which gray represents the PVC substrate, blue represents the SA hydrogel coating, and yellow represents the AMP-embedded hydrogel coating.

performed in at least three parallel samples. The measured experimental results were compared with nonparametric ANOVA tests using SPSS software, and statistical significance on the basis of the p value was less than 0.05.

3. RESULTS AND DISCUSSION

3.1. Characterization of the Hydrogel Coating. The fabrication process of the AMP-embedded hydrogel coating is schematically illustrated in Scheme 1. The PVC catheter was first treated with benzophenone and then immersed into a monomer solution. After irradiation under UV for 1 h, a thin and robust hydrogel layer was generated on the PVC tube; using the same method, hydrogel coatings were also prepared with PDMS and a polyurethane substrate, as reported in our previous research.[48] The surface-initiated polymerization mechanism is described as follows. Due to the dehydrogenation of benzophenone, active free radicals formed in the PVC polymer backbone could initiate the polymerization of the monomers under UV irradiation. Thus, poly(SBMA-co-AAc) contained zwitterions and carboxyl anions that were chemically grafted onto the PVC backbone, which might offer the hydrogel with good hemocompatibility and antifouling properties. Subsequently, AMPs were then grafted onto the hydrogel coating to endow antibacterial properties. The amount of AMPs loaded in the hydrogels was 4.5 ± 0.8 and 3.5 ± 0.9 μg/cm^2 for WR and Bac2A, respectively.

Homogeneity, coverage, and stability were essential parameters for surface coating. As shown in Figure 1A, after staining with toluidine blue, the hydrogel coating fully and homogenously covered the inside of the tube surface. Moreover, after immersion into water, the hydrogel-coated tube showed a very distinct color from the bare tube. As shown in Figure 1B and Figure S1, a thin hydrogel layer was clearly observed under an optical microscope, which could swell in water. SEM was chosen to further characterize the surface topography of the hydrogel coating. As shown in Figure 1C, SA (poly(SMBA-co-AAc) hydrogel coating) displayed a wrinkled surface topography under a low magnification, in accordance with the previous report.[48] After peptide grafting, the surface topography changed slightly due to the weak cross-link. The cross-sectional images of the hydrogel coating are shown in Figure 1D and Figure S2; under a high magnification, a thin hydrogel layer containing some micropores was observed. Luckily, no stripping gap was observed because the coated hydrogel was chemically grafted onto the PVC backbone. The thickness of different samples was determined using an optical microscope. As shown in Figure 1E, the thickness of SA was 40 μm under dry conditions, but it can swell to 70 μm. The thicknesses of SA-WR (the hydrogel coating grafted with AMP WR (amino acid sequence: WRWRWR-NH2)) and SA-Bac2A (the hydrogel coating grafted with AMP WR (amino acid sequence: RLARIVVIR-VAR-NH2)) were around 60 μm, and they could swell to 75 μm. The grafted AMPs increased the hydrogel coating thickness but reduced the swelling ratio probably because the ion interaction between AMPs and AAc weakened the water absorption (Figure S3). As shown in Figure 1F and Figure S4, no obvious weight loss was detected after immersing

https://doi.org/10.1021/acsami.1c05167
ACS Appl. Mater. Interfaces 2021, 13, 38947–38958

the hydrogel coating into PBS for 4 weeks, indicating its good stability. As can be seen from Figure 1G, the PVC tube exhibited a hydrophobic surface with 90° WCA. After coated with the SA hydrogel, the static WCA decreased to 27° due to the abundant hydrophilic groups. After AMP grafting, the static WCAs of SA-WR and SA-Bac2A increased over 100° with clearly contact angle hysteresis around 30−32°. The receding contact angles of both AMP-embedded hydrogels were around 43°, indicating their good wettability. As shown in Figure 1H, the negatively charged PVC tube with a zeta potential of −37 mV changed to neutral after being coated with the SA hydrogel. After AMP grafting, the zeta potentials changed slightly and were −3 and −5 mV for SA-WR and SA-Bac2A, respectively.

Figure 2A and Figure S5 show the FTIR spectra of the hydrogel coatings. For the PVC sample, the peak at 1720 cm^{-1} was assigned to the characteristic vibrations of carbonyl groups of parabens, which was used as a PVC-processing additive. After immobilizing the SA hydrogel, a new peak at 1039 cm^{-1} ascribed to the $-SO_3^-$ group appeared in the FTIR spectrum of the SA sample. After AMP grafting, new peaks at 1600 and 1650 cm^{-1} appeared, corresponding to the vibrations of N−H of the amide group. The surface elemental compositions were confirmed by XPS spectra shown in Figure 2B,C. It could be seen that the pristine PVC showed no peak around 402.3 and 168.5 eV due to the lack of N and S elements. However, after coating with the SA hydrogel, two strong peaks at around 402.3 and 168.5 eV were clearly observed, which could be attributed to N 1s ($C-N^+$) and S 2p (SO_3^-), respectively. After AMP grafting, the N 1s signal could be deconvoluted into two separate peaks at 399.8 and 402.3 eV, respectively, in which the peak at 399.8 eV was attributed to the nitrogen of primary amine groups and amide of AMPs. The XPS results indicated that AMPs were embedded in the SA hydrogel coating with a dotted distribution instead of a fully covered layer, which was expected to retain the antithrombus and antifouling properties of the SA hydrogel. The element distribution was further tested by EDS, and the results are shown in Figure 2G−I and Figure S6. The element distributions of Na, S, and N were detected along with the white line marked in Figure 2D−F. For the SA sample, the Na element, representing the AAc block in the polymer, appeared and had a depth of about 100 μm and the PVC side was 100 μm. Meanwhile, the S element, representing the SBMA block in the polymer, appeared and had a depth of about 50 μm. These results indicated that the content of the AAc block was almost same as that of SBMA at the top of the hydrogel coating but exceeded that of SBMA at the interface between the hydrogel coating and the PVC substrate. This hierarchical structure was also observed in SA-WR and SA-Bac2A samples (PVC side was 200 μm). The existing N elements indicated the chemically attached AMPs. More interestingly, the N element showed a gradient distribution probably because the positively charged AMPs formed a "shell" after interaction with the negatively charged poly(SBMA-co-AAc) and thus it was hard for their deep permeation. Thus, the AMPs were just attached at the "upper surface" of the hydrogel coating, instead of being fully and deeply attached into the hydrogel coating. The detection of Na and S further indicated that the AMPs were embedded in the "upper surface" of the hydrogel coating surface with a dotted distribution, as shown in Figure 2H,I. Importantly, this structure would be beneficial for biomedical applications, as shown in Figure 3. On the one hand, the

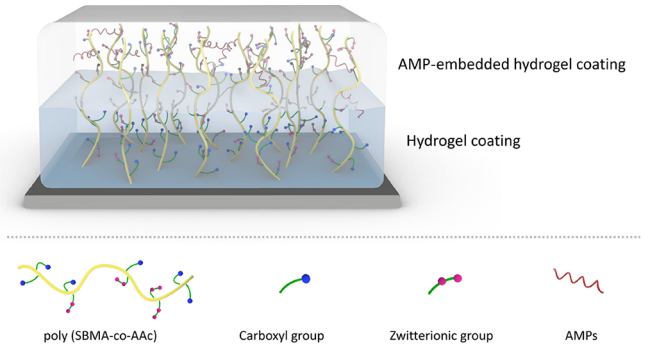

Figure 3. Proposed chemical structure of the AMP-embedded hydrogel coating.

embedded AMPs could endow the hydrogel coating's antibacterial ability with reserving antithrombus and antifouling properties of the hydrogel coating due to the dotted distribution of AMPs. On the other hand, the hydrogel coating could protect the bioactivity of AMPs for a long time and cover the positive charge of AMPs, which was unfavorable for hemocompatibility and antifouling ability.

3.2. Anticoagulant Performance of the Hydrogel Coating. Hemocompatibility is essential for a blood-contacting catheter. During the use of a blood-contacting device, platelets and other blood cells should not adhere to the surface because the adhered platelet would undergo a series of activating reactions that could cause blood clotting and thrombosis. Herein, the adhesion of blood cells on the surfaces was investigated. The samples were immersed in fresh PRP, and the attached platelets were observed using a SEM. As shown in Figure 4A, abundant platelets adhered on the surface of pristine PVC while few platelets adhered to the surfaces of SA, SA-WR, and SA-Bac2A. The semi-quantitative analysis of platelet adhesion on the surface was carried out using LDH released from the platelets. The LDH activity was evaluated using OD. As shown in Figure 4B, compared to that of pristine PVC (1.081), the OD values of SA-WR and SA-Bac2A coatings decreased to 0.256 and 0.342, respectively. Moreover, the results of the hemolytic assay shown in Figure 4C indicated that the hemolysis ratios of all the samples were less than 5%, demonstrating their good hemocompatibility. The increased hemolysis ratio of SA-WR could be attributed to the embedded WR, which has more hydrophobic indole rings of tryptophan. Luckily, the hemolysis ratio was still less than 5%. In vitro cytotoxicity of the sample leachate was evaluated with HUVECs (Figure S7). The relative cell viability of each group was higher than 75%, indicating that all samples possessed good cytocompatibility. These results suggested that the antibacterial functionalization did not exert negative effects on the biocompatibility of PVC. Therefore, this hydrogel coating with biocompatible components including hydrophilic and negatively charged polymers as well as nonreleased AMP could be applied for antibacterial functionalization of blood-related medical devices.

To further evaluate the antithrombogenic properties of SA, SA-WR, and SA-Bac2A, an ex vivo perfusion experiment was performed using an arteriovenous shunt model in rabbit (Figure 4D). After 2 h of ex vivo circulation in the arteriovenous shunts, the circuit of bare PVC displayed an obvious blood streak while those of the hydrogel-coated samples were clean (Figure 4E). According to the SEM result shown in Figure 4F, the internal surface of the SA tube could

https://doi.org/10.1021/acsami.1c05167
ACS Appl. Mater. Interfaces 2021, 13, 38947−38958

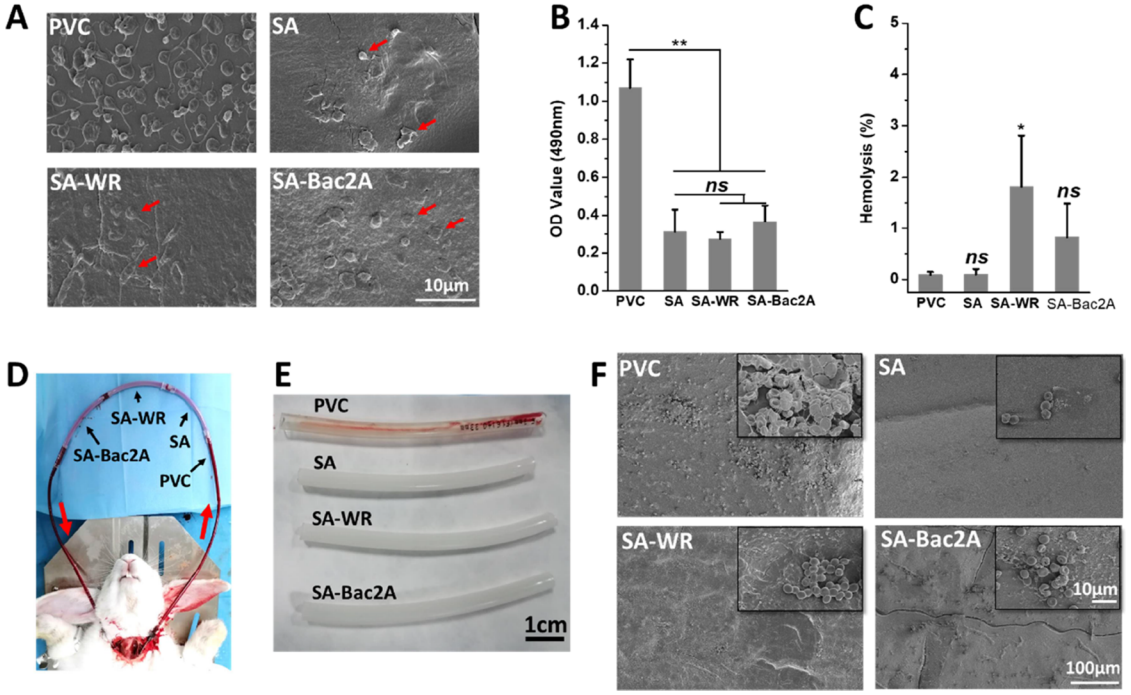

Figure 4. (A) Representative SEM images of platelet adhesion; the red arrows indicate the adhesive platelets. (B) Semi-quantitative analysis of platelet adhesion onto the sample surface using the LDH assay kit. The LDH content could be used to estimate the amount of adhesive platelets (**$p < 0.01$, *ns* = no significant difference ($p > 0.05$), mean ± SD, $n = 3$). (C) Hemolytic ability of pristine PVC, SA, SA-WR, and SA-Bac2A (* $p < 0.05$, *ns* = no significant difference ($p > 0.05$), mean values ± SD, $n = 3$). (D) Ex vivo test using a New Zealand white rabbit. (E) Digital photograph of bare PVC, SA, SA-WR, and SA-Bac2A after 2 h of ex vivo circulation. (F) SEM view of the thrombus deposition on different samples after the ex vivo perfusion experiment.

efficiently inhibit the formation of thrombi with only a few RBCs found, mainly due to their antifouling and antithrombus properties. The internal surfaces of SA-WR and SA-Bac2A tubes were as clean as the SA tube with only few platelets and RBCs. However, several thrombi were observed on the surface of the uncoated PVC tube. The ex vivo tests further confirmed that the hydrogel coatings possessed excellent hemocompatibility and antithrombus properties.

3.3. Antibacterial and Antifouling Properties of the Hydrogel Coating. The foreign body-related infections were initiated by the transport of bacteria toward the substratum surface and subsequent attachment. Typical Gram-positive bacteria *S. aureus* and Gram-negative bacteria *E. coli* were used to evaluate the antibacterial and antifouling potentials of SA, SA-WR, and SA-Bac2A hydrogel coatings. As shown in Figure 5A−C, bacteria collected from pristine PVC grew into colonies on agar plates with *E. coli* and *S. aureus* of $(6.21 \pm 0.6) \times 10^4$ and $(4.32 \pm 0.5) \times 10^4$ CFU/cm^2, respectively. In addition, bacteria collected from SA grew into colonies on agar plates with *E. coli* and *S. aureus* of $(5.41 \pm 0.5) \times 10^4$ and $(4.65 \pm 0.5) \times 10^4$ CFU/cm^2, respectively. No colony was found on the plates spread with bacteria collected from SA-WR and SA-Bac2A, suggesting their excellent antibacterial activities due to the bioactivity of chemically grafted AMPs in the initial stage.

As a novel antimicrobial antibiotic, the stability of AMPs raised much concerns during surface modification. As shown in Figure 1F, the weights of SA-WR and SA-Bac2A were almost unchanged after 4 weeks of immersion in PBS at 37 °C, indicating their excellent stability. The long-term antibacterial properties were further tested with the contact-killing method. As shown in Figure 5D−F, after immersing in PBS for 4 weeks and only then challenging with bacteria, SA-Bac2A could still display a strong antibacterial action against *E. coli* and *S. aureus*. All the bacteria were killed after contacting with the SA-Bac2A surface. However, the antibacterial function of SA-WR showed a little decrease based on the observation of some colonies on the surface of the medium. Overall, SA-Bac2A exhibited a superior and long-term bioactive stability, which could be attributed to the protection of the hydrogel coating. Moreover, even after storing under dry conditions for 4 weeks, both SA-WR and SA-Bac2A still exhibited excellent antibacterial properties, as shown in Figure S8.

Meanwhile, *S. aureus* and *E. coli* were used to evaluate the antifouling properties of the samples in MH medium. The adhered bacteria on the surface were assessed using the CLSM images shown in Figure 5G,H in which live bacteria were labeled with green fluorescence and dead bacteria were labeled with red. It could be seen that a large amount of live bacteria and few dead bacteria were observed on the surface of PVC. Both live and dead bacteria adhered on the surface of SA, SA-WR, and SA-Bac2A were significantly reduced, demonstrating their excellent antifouling properties. This was because the zwitterionic SBMA in the hydrogel coating could bind more "free water," which could effectively prevent bacterial adhesion. Furthermore, the embedded positively charged AMPs did not influence the antifouling properties of the hydrogel coating due to the weak change in zeta potential and wettability as shown in Figure 1G,H. Thus, the AMP-embedded hydrogel coating possessed both contact-killing and antifouling properties.

3.4. In Vivo Biocompatibility and Anti-Infection Evaluation. To assess the in vivo antibacterial properties, an animal model associated with catheter-induced infections was established (Figure 6A). The implanted samples were contaminated with *S. aureus* suspension. After 1 and 3 days,

https://doi.org/10.1021/acsami.1c05167
ACS Appl. Mater. Interfaces 2021, 13, 38947−38958

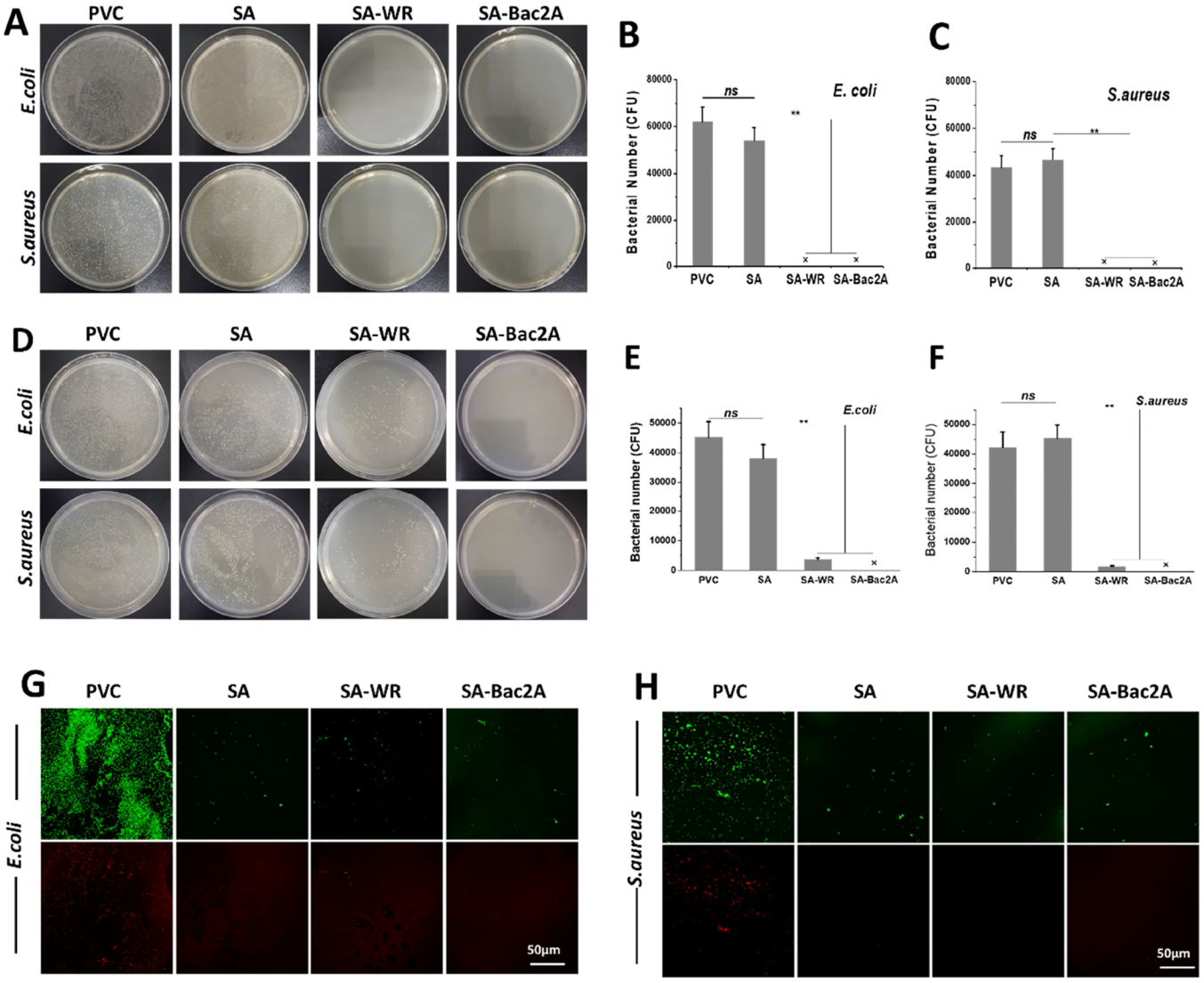

Figure 5. (A) Photographs and (B, C) the numbers of corresponding *E. coli* and *S. aureus* bacterial colonies on agar plates that eluted from the PVC, SA, SA-WR, and SA-Bac2A samples (**$p < 0.01$, *ns* = no significant difference ($p > 0.05$), cross symbol indicating no live bacteria, mean values ± SD, $n = 6$). (D) Photographs and (E, F) the numbers of corresponding *E. coli* and *S. aureus* bacterial colonies on agar plates that eluted from the PVC, SA, SA-WR, and SA-Bac2A samples. All samples were immersed into PBS for 4 weeks and only afterward incubated with the bacteria (** $p < 0.01$, *ns* = no significant difference ($p > 0.05$), cross symbol indicating no live bacteria, mean values ± SD, $n = 6$). (G, H) CLSM images of the PVC, SA, SA-WR, and SA-Bac2A samples after incubating with *E. coli* and *S. aureus*.

the implanted samples were collected to quantify the bacterial numbers. As shown in Figure 6B–D, a large amount of bacterial cells were found on the surface of pristine PVC and SA. In contrast, only few bacteria survived on the surfaces of SA-WR and SA-Bac2A. The animal experimental results demonstrated that SA-WR and SA-Bac2A could effectively kill bacteria in vivo due to their good antibacterial properties.

In addition, the surrounding tissue was subjected to H&E staining, as shown in Figure 6E. Prominent neutrophilic infiltration was observed at day 1 and day 3 in PVC and SA groups, indicating an acute inflammatory response induced by bacterial infection. In contrast, infiltration of inflammation cells dramatically decreased in SA-WR and SA-Bac2A groups, indicating that the bacterial infection was effectively inhibited. The phenotype of inflammatory cells surrounding the implants was further analyzed by biological markers. As can be seen from Figure 7, most cells around the explants were CD68-marked macrophage cells and CD3-marked T cells for PVC and SA. For SA-WR and SA-Bac2A samples, the macrophage cell and T cell numbers were low than those for the PVC and SA groups, and no significant difference was observed between SA-WR and SA-Bac2A groups. These results indicated the AMP-embedded hydrogel coating could reduce the inflammatory response by killing the infected bacteria. Moreover, positively charged AMPs being encapsulated in the hydrogel would not cause the inflammatory response. Thus, the AMP-embedded hydrogel coating exhibited both good antibacterial and anti-inflammatory properties in vivo.

4. CONCLUSIONS

In summary, a novel strategy was developed to endow blood-contacting devices and related implant surfaces with integrated antibacterial and antithrombus properties. The AMP-embedded hydrogel coating was constructed on a polymeric substrate through surface-initiated polymerization, which possessed excellent antithrombus, antifouling, and antibacterial properties

https://doi.org/10.1021/acsami.1c05167
ACS Appl. Mater. Interfaces 2021, 13, 38947−38958

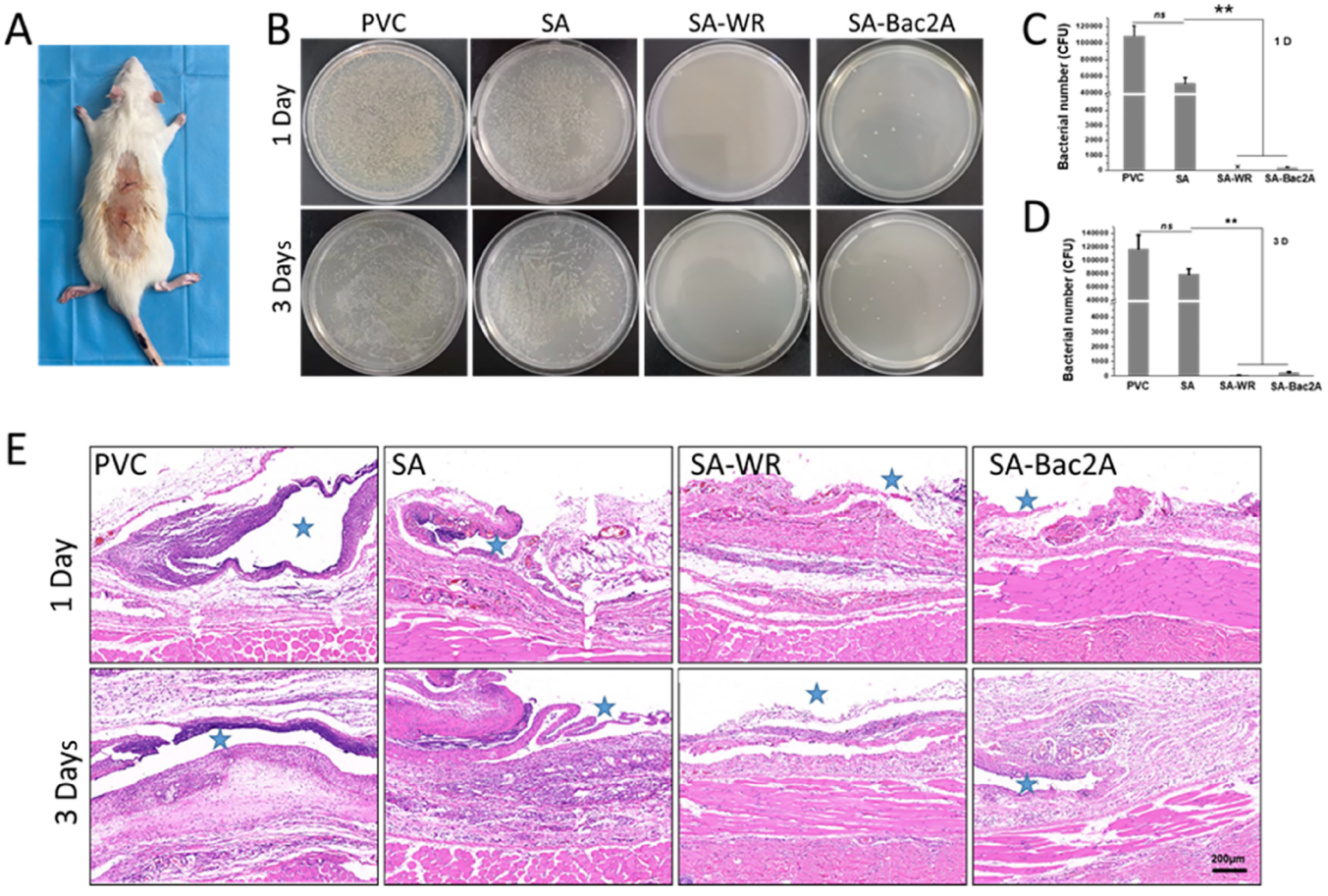

Figure 6. (A) Animal model associated with catheter-induced infections. Samples were implanted into the back of SD rats, and then *S. aureus* suspensions were injected into the hydrogel coating surface. (B) Photographic images and (C, D) the corresponding bacterial numbers of *S. aureus* on agar plates, ultrasonically removed from the sample surfaces after 1 and 3 days of implantation (** $p < 0.01$, *ns* = no significant difference ($p > 0.05$), mean values ± SD, $n = 6$). (E) H&E staining assay of the sample-contacted tissue. The implanted catheter was indicated with a blue star.

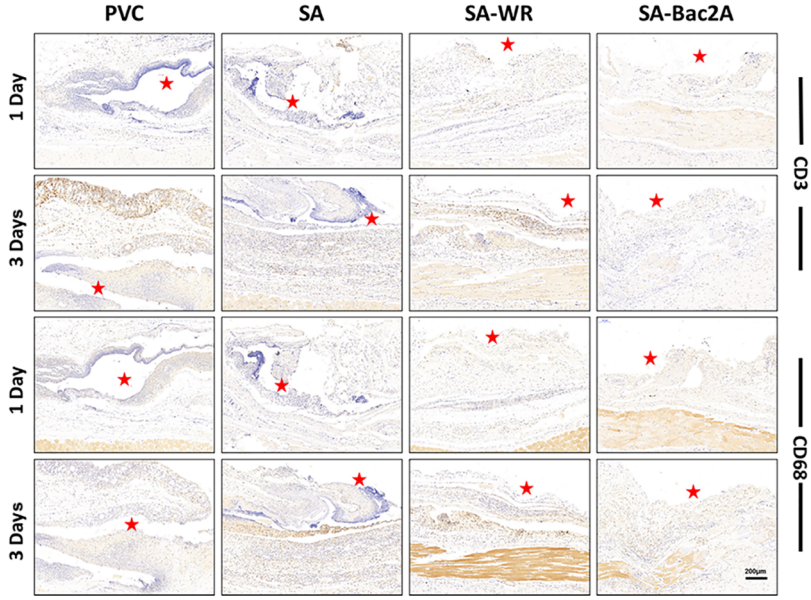

Figure 7. CD3 and CD68 staining assays of the implanted catheter-contacted tissue. The implanted catheter was infected with *S. aureus* for 1 and 3 days. The implanted catheter was indicated with a red star for CD68-marked macrophage cells and CD3-marked T cells.

with stable bioactivity for a long time. Ex vivo experiments confirmed the antithrombus ability of the hydrogel coating. Furthermore, both SA-WR and SA-Bac2A showed excellent bactericidal and antiadhesion properties against Gram-positive and Gram-negative bacteria. More importantly, the bactericidal properties of SA-Bac2A were retained after immersing into

https://doi.org/10.1021/acsami.1c05167
ACS Appl. Mater. Interfaces 2021, 13, 38947−38958

PBS for 4 weeks. The anti-infection performance in vivo was verified through the microbiological and histological results of animal experiments. Immunohistological analysis data further indicated that the hydrogel coating has a good anti-inflammatory function. The present study shows the promising clinical application potential in preventing bacterial infection and thrombosis for blood-contacting medical devices and related implants.

■ ASSOCIATED CONTENT

Supporting Information

The Supporting Information is available free of charge at https://pubs.acs.org/doi/10.1021/acsami.1c05167.

Microphotograph of the sectional view of the hydrogel coating (Figure S1), SEM images of the cross section of the hydrogel coating (Figure S2), water absorption ability of PVC and hydrogel-coated samples (Figure S3), scratching test of the hydrogel coating using a steel tweezer (Figure S4), FTIR spectra of samples (Figure S5), map scanning of different hydrogel coatings in a section view by EDS (Figure S6), cell viability of HUVECs (Figure S7), *E. coli* and *S. aureus* colonies on agar plates from the samples (Figure S8), and XPS data of the coatings (Table S1) (PDF)

■ AUTHOR INFORMATION

Corresponding Authors

Li Yang − *National Engineering Research Center for Biomaterials, Sichuan University, Chengdu 610064, China;* orcid.org/0000-0003-0456-4041; Email: yanglisc@scu.edu.cn

Rifang Luo − *National Engineering Research Center for Biomaterials, Sichuan University, Chengdu 610064, China;* orcid.org/0000-0002-8998-9948; Email: lrifang@scu.edu.cn

Authors

Kunpeng Liu − *National Engineering Research Center for Biomaterials, Sichuan University, Chengdu 610064, China*

Fanjun Zhang − *National Engineering Research Center for Biomaterials, Sichuan University, Chengdu 610064, China*

Yuan Wei − *National Engineering Research Center for Biomaterials, Sichuan University, Chengdu 610064, China*

Qinsheng Hu − *West China Hospital, Sichuan University, Chengdu 610064, China*

Qingfeng Luo − *Center for Medical Device Evaluation of NMPA, Beijing 100081, China*

Chong Chen − *Laboratory of Biomechanical Engineering, Department of Applied Mechanics, College of Architecture & Environment, Sichuan University, Chengdu 610064, China*

Jingyu Wang − *First Affiliated Hospital of Xi'an Jiaotong University, Xi'an 710061, China*

Yunbing Wang − *National Engineering Research Center for Biomaterials, Sichuan University, Chengdu 610064, China;* orcid.org/0000-0002-2412-6762

Complete contact information is available at: https://pubs.acs.org/10.1021/acsami.1c05167

Author Contributions

#K.L. and F.Z. contributed equally to this article.

Notes

The authors declare no competing financial interest.

■ ACKNOWLEDGMENTS

This work was supported by the funding listed as follows: the Sichuan Science and Technology Program (2021YFH0011), the National Key Research and Development Program (2016YFC1102200), the 111 Project (the Program of Introducing Talents of Discipline to Universities (B16033)), the Initiation Funding for Interdisciplinary Research of Sichuan University (No. 0040204153251), and the Sichuan Science and Technology Major Project (2018SZDZX0011).

■ REFERENCES

(1) Cosgrove, S. E.; Qi, Y. L.; Kaye, K. S.; Harbarth, S.; Karchmer, A. W.; Carmeli, Y. The Impact of Methicillin Resistance inStaphylococcus aureusBacteremia on Patient Outcomes: Mortality, Length of Stay, and Hospital Charges. *Infect Control Hosp Epidemiol* **2005**, *26*, 166−174.

(2) Rehman, S.; Ansari, M. A.; Buhaimed, A.; Ibrahim, F.; Gani, A. Colonization Frequency, Endophytic Infection Rate and Bioactivities of Microbes of Desert Medicinal Plants. *J. Chem. Soc. Pakistan* **2019**, *41*, 501−508.

(3) Ariza-Heredia, E. J.; Chemaly, R. F. Update on Infection Control Practices in Cancer Hospitals. *Ca-Cancer J. Clin.* **2018**, *68*, 340−355.

(4) Jaffer, I. H.; Weitz, J. I. The blood compatibility challenge. Part 1: Blood-contacting medical devices: The scope of the problem. *Acta Biomater.* **2019**, *94*, 2−10.

(5) Alban, S. Adverse effects of heparin. *Handb. Exp. Pharmacol.* **2012**, *207*, 211−263.

(6) Cohen, M. L. Epidemiology of drug resistance: implications for a post-antimicrobial era. *Science* **1992**, *257*, 1050−1055.

(7) Chen, S. S.; Wang, H.; Katzianer, D. S.; Zhong, Z. T.; Zhu, J. LysR family activator-regulated major facilitator superfamily transporters are involved in Vibrio cholerae antimicrobial compound resistance and intestinal colonisation. *Int. J. Antimicrob. Ag.* **2013**, *41*, 188−192.

(8) Ding, X. K.; Duan, S.; Ding, X. J.; Liu, R. H.; Xu, F. J. Versatile Antibacterial Materials: An Emerging Arsenal for Combatting Bacterial Pathogens. *Adv. Funct. Mater.* **2018**, *28*, No. 1802140.

(9) Hasan, J.; Crawford, R. J.; Lvanova, E. P. Antibacterial surfaces: the quest for a new generation of biomaterials. *Trends Biotechnol.* **2013**, *31*, 295−304.

(10) Yang, H. T.; Li, G. F.; Stansbury, J. W.; Zhu, X. Q.; Wang, X.; Nie, J. Smart Antibacterial Surface Made by Photopolymerization. *ACS Appl. Mater. Interfaces* **2016**, *8*, 28047−28054.

(11) Jalvo, B.; Faraldos, M.; Bahamonde, A.; Rosal, R. Antibacterial surfaces prepared by electrospray coating of photocatalytic nanoparticles. *Chem. Eng. J.* **2018**, *334*, 1108−1118.

(12) Moritz, M.; Geszke-Moritz, M. The newest achievements in synthesis, immobilization and practical applications of antibacterial nanoparticles. *Chem. Eng. J.* **2013**, *228*, 596−613.

(13) Liu, S.; Guo, W. W. Anti-Biofouling and Healable Materials: Preparation, Mechanisms, and Biomedical Applications. *Adv. Funct. Mater.* **2018**, *28*, No. 1800596.

(14) Chen, S. Q.; Xie, Y.; Xiao, T. J.; Zhao, W. F.; Li, J. S.; Zhao, C. S. Tannic acid-inspiration and post-crosslinking of zwitterionic polymer as a universal approach towards antifouling surface. *Chem. Eng. J.* **2018**, *337*, 122−132.

(15) Zhao, X. Y.; Yang, J. H.; Liu, Y.; Gao, J. S.; Wang, K.; Liu, W. G. An injectable and antifouling self-fused supramolecular hydrogel for preventing postoperative and recurrent adhesions. *Chem. Eng. J.* **2021**, *404*, No. 127096.

(16) Lv, J. L.; Zhang, G. Q.; Zhang, H. M.; Yang, F. L. Graphene oxide-cellulose nanocrystal (GO-CNC) composite functionalized PVDF membrane with improved antifouling performance in MBR: Behavior and mechanism. *Chem. Eng. J.* **2018**, *352*, 765−773.

(17) Zhang, Y. Z.; Liu, X. M.; Li, Z. Y.; Zhu, S. L.; Yuan, X. B.; Cui, Z. D.; Yang, X. J.; Chu, P. K.; Wu, S. L. Nano Ag/ZnO-Incorporated Hydroxyapatite Composite Coatings: Highly Effective Infection

Prevention and Excellent Osteointegration. *ACS Appl. Mater. Interfaces* **2018**, *10*, 1266−1277.
(18) Yoosefi Booshehri, A.; Wang, R.; Xu, R. The effect of regenerable silver nanoparticles/multi-walled carbon nanotubes coating on the antibacterial performance of hollow fiber membrane. *Chem. Eng. J.* **2013**, *230*, 251−259.
(19) Huang, L. Y.; Lou, Y. T.; Zhang, D. W.; Ma, L. W.; Qian, H. C.; Hu, Y. T.; Ju, P. F.; Xu, D. K.; Li, X. G. D-Cysteine functionalised silver nanoparticles surface with a ″disperse-then-kill″ antibacterial synergy. *Chem. Eng. J.* **2020**, *381*, No. 122662.
(20) Huang, N. M.; Radiman, S.; Lim, H. N.; Khiew, P. S.; Chiu, W. S.; Lee, K. H.; Syahida, A.; Hashim, R.; Chia, C. H. γ-Ray assisted synthesis of silver nanoparticles in chitosan solution and the antibacterial properties. *Chem. Eng. J.* **2009**, *155*, 499−507.
(21) Budama, L.; Çakır, B. A.; Topel, Ö.; Hoda, N. A new strategy for producing antibacterial textile surfaces using silver nanoparticles. *Chem. Eng. J.* **2013**, *228*, 489−495.
(22) Wu, V. M.; Tang, S.; Uskokovic, V. Calcium Phosphate Nanoparticles as Intrinsic Inorganic Antimicrobials: The Antibacterial Effect. *ACS Appl. Mater. Interfaces* **2018**, *10*, 34013−34028.
(23) Geng, C.; Liang, Z.; Cui, F.; Zhao, Z.; Yuan, C.; Du, J.; Wang, C. Energy-saving photo-degradation of three fluoroquinolone antibiotics under VUV/UV irradiation: Kinetics, mechanism, and antibacterial activity reduction. *Chem. Eng. J.* **2020**, *383*, No. 123145.
(24) Lei, J.; Chen, B.; Zhou, L.; Ding, N.; Cai, Z.; Wang, L.; In, S.-I.; Cui, C.; Zhou, Y.; Liu, Y.; Zhang, J. Efficient degradation of antibiotics in different water matrices through the photocatalysis of inverse opal K-g-C3N4: Insights into mechanism and assessment of antibacterial activity. *Chem. Eng. J.* **2020**, *400*, No. 125902.
(25) Zhang, Y. Q.; Hudson-Smith, N. V.; Frand, S. D.; Cahill, M. S.; Davis, L. S.; Feng, Z. V.; Haynes, C. L.; Hamers, R. J. Influence of the Spatial Distribution of Cationic Functional Groups at Nanoparticle Surfaces on Bacterial Viability and Membrane Interactions. *J. Am. Chem. Soc.* **2020**, *142*, 10814−10823.
(26) Li, M.-S.; Zhao, Z.-P.; Wang, M.-X.; Zhang, Y. Controllable modification of polymer membranes by LDDLT plasma flow: Antibacterial layer onto PE hollow fiber membrane module. *Chem. Eng. J.* **2015**, *265*, 16−26.
(27) Chen, Y.; Ding, Y.; Zheng, J. A polymer nanocomposite coating with enhanced hydrophilicity, antibacterial and antibiofouling properties: Role of polymerizable emulsifier/anionic ligand. *Chem. Eng. J.* **2020**, *379*, No. 122268.
(28) Li, X.; Hu, X. F.; Cai, T. Construction of Hierarchical Fouling Resistance Surfaces onto Poly(vinylidene fluoride) Membranes for Combating Membrane Biofouling. *Langmuir* **2017**, *33*, 4477−4489.
(29) Ippel, B. D.; Dankers, P. Y. W. Introduction of Nature's Complexity in Engineered Blood-compatible Biomaterials. *Adv. Healthc. Mater.* **2018**, *7*, No. 1700505.
(30) Samav, Y.; Akpinar, B.; Kocak, G.; Butun, V. Preparation of Responsive Zwitterionic Diblock Copolymers Containing Phosphate and Phosphonate Groups. *Macromol. Res.* **2020**, *28*, 1134−1141.
(31) Wang, W.; Lu, Y.; Zhu, H.; Cao, Z. Superdurable Coating Fabricated from a Double-Sided Tape with Long Term ″Zero″ Bacterial Adhesion. *Adv. Mater.* **2017**, *29*, No. 1606506.
(32) Wang, G.; Wang, L.; Lin, W.; Wang, Z.; Zhang, J.; Ji, F.; Ma, G.; Yuan, Z.; Chen, S. Development of Robust and Recoverable Ultralow-Fouling Coatings Based on Poly(carboxybetaine) Ester Analogue. *ACS Appl. Mater. Interfaces* **2015**, *7*, 16938−16945.
(33) Zhu, M. M.; Fang, Y.; Chen, Y. C.; Lei, Y. Q.; Fang, L. F.; Zhu, B. K.; Matsuyama, H. Antifouling and antibacterial behavior of membranes containing quaternary ammonium and zwitterionic polymers. *J. Colloid Interface Sci.* **2021**, *584*, 225−235.
(34) Tiller, J. C.; Liao, C. J.; Lewis, K.; Klibanov, A. M. Designing surfaces that kill bacteria on contact. *Proc. Natl. Acad. Sci. USA* **2001**, *98*, 5981−5985.
(35) Stirling, F.; Bitzan, L.; O'Keefe, S.; Redfield, E.; Oliver, J. W. K.; Way, J.; Silver, P. A. Rational Design of Evolutionarily Stable Microbial Kill Switches. *Mol. Cell* **2017**, *68*, 686−697.e3.
(36) Borjihan, Q.; Dong, A. Design of nanoengineered antibacterial polymers for biomedical applications. *Biomater. Sci.* **2020**, *8*, 6867−6882.
(37) Liu, L.; Shi, H.; Yu, H.; Yan, S.; Luan, S. Correction: The recent advances in surface antibacterial strategies for biomedical catheters. *Biomater. Sci.* **2020**, *8*, 4638−4638.
(38) Ghasemlou, M.; Daver, F.; Ivanova, E. P.; Rhim, J. W.; Adhikari, B. Switchable Dual-Function and Bioresponsive Materials to Control Bacterial Infections. *ACS Appl. Mater. Interfaces* **2019**, *11*, 22897−22914.
(39) Li, L. H.; Yang, L.; Liao, Y. B.; Yu, H. C.; Liang, Z.; Zhang, B.; Lan, X. R.; Luo, R. F.; Wang, Y. B. Superhydrophilic versus normal polydopamine coating: A superior and robust platform for synergistic antibacterial and antithrombotic properties. *Chem. Eng. J.* **2020**, *402*, No. 126196.
(40) Liu, Y. N.; Li, F.; Guo, Z. R.; Xiao, Y. Q.; Zhang, Y. L.; Sun, X. Y.; Zhe, T. T.; Cao, Y. Y.; Wang, L.; Lu, Q. Y.; Wang, J. H. Silver nanoparticle-embedded hydrogel as a photothermal platform for combating bacterial infections. *Chem. Eng. J.* **2020**, *382*, No. 122990.
(41) Carratala, J. V.; Serna, N.; Villaverde, A.; Vazquez, E.; Ferrer-Miralles, N. Nanostructured antimicrobial peptides: The last push towards clinics. *Biotechnol. Adv.* **2020**, *44*, No. 107603.
(42) Magana, M.; Pushpanathan, M.; Santos, A. L.; Leanse, L.; Fernandez, M.; Ioannidis, A.; Giulianotti, M. A.; Apidianakis, Y.; Bradfute, S.; Ferguson, A. L.; Cherkasov, A.; Seleem, M. N.; Pinilla, C.; de la Fuente-Nunez, C.; Lazaridis, T.; Dai, T. H.; Houghten, R. A.; Hancock, R. E. W.; Tegos, G. P. The value of antimicrobial peptides in the age of resistance. *Lancet Infect. Dis.* **2020**, *20*, E216−E230.
(43) Brogden, K. A. Antimicrobial peptides: Pore formers or metabolic inhibitors in bacteria? *Nat. Rev. Microbiol.* **2005**, *3*, 238−250.
(44) Bagheri, M.; Beyermann, M.; Dathe, M. Immobilization Reduces the Activity of Surface-Bound Cationic Antimicrobial Peptides with No Influence upon the Activity Spectrum. *Antimicrob. Agents Ch.* **2009**, *53*, 1132−1141.
(45) Cheng, G.; Mi, L.; Cao, Z. Q.; Xue, H.; Yu, Q. M.; Carr, L.; Jiang, S. Y. Functionalizable and Ultrastable Zwitterionic Nanogels. *Langmuir* **2010**, *26*, 6883−6886.
(46) Mi, L.; Jiang, S. Integrated antimicrobial and nonfouling zwitterionic polymers. *Angew. Chem. Int. Ed. Engl.* **2014**, *53*, 1746−1754.
(47) Liang, Y.; Zhang, X.; Yuan, Y.; Bao, Y.; Xiong, M. Role and modulation of the secondary structure of antimicrobial peptides to improve selectivity. *Biomater. Sci.* **2020**, *8*, 6858−6866.
(48) Zhang, F.; Hu, C.; Yang, L.; Liu, K.; Ge, Y.; Wei, Y.; Wang, J.; Luo, R.; Wang, Y. A conformally adapted all-in-one hydrogel coating: towards robust hemocompatibility and bactericidal activity. *J. Mater. Chem. B* **2021**, *9*, 2697−2708.
(49) Parada, G.; Yu, Y.; Riley, W.; Lojovich, S.; Tshikudi, D.; Ling, Q.; Zhang, Y.; Wang, J.; Ling, L.; Yang, Y.; Nadkarni, S.; Nabzdyk, C.; Zhao, X. Ultrathin and Robust Hydrogel Coatings on Cardiovascular Medical Devices to Mitigate Thromboembolic and Infectious Complications. *Adv. Healthc. Mater.* **2020**, *9*, No. 2001116.
(50) Zhao, C.; Zhou, L.; Chiao, M.; Yang, W. Antibacterial hydrogel coating: Strategies in surface chemistry. *Adv. Colloid Interface Sci.* **2020**, *285*, No. 102280.
(51) Lu, J.; Zhuang, W.; Li, L.; Zhang, B.; Yang, L.; Liu, D.; Yu, H.; Luo, R.; Wang, Y. Micelle-embedded layer-by-layer coating with catechol and phenylboronic acid for tunable drug loading, sustained release, mild tissue response, and selective cell fate for re-endothelialization. *ACS Appl. Mater. Interfaces* **2019**, *11*, 10337−10350.
(52) Zhao, Y.; Wei, B. L.; Wu, M.; Zhang, H. L.; Yao, J. R.; Chen, X.; Shao, Z. Z. Preparation and characterization of antibacterial poly(lactic acid) nanocomposites with N-halamine modified silica. *Int. J. Biol. Macromol.* **2020**, *155*, 1468−1477.
(53) Hu, C.; Zhang, F.; Kong, Q.; Lu, Y.; Zhang, B.; Wu, C.; Luo, R.; Wang, Y. Synergistic Chemical and Photodynamic Antimicrobial Therapy for Enhanced Wound Healing Mediated by Multifunctional

Light-Responsive Nanoparticles. *Biomacromolecules* **2019**, *20*, 4581−4592.

https://doi.org/10.1021/acsami.1c05167
ACS Appl. Mater. Interfaces 2021, 13, 38947−38958